Structural Characterization and Reversal of the Natural Organophosphate Resistance of a D-Type Esterase, *Saccharomyces cerevisiae S*-Formylglutathione Hydrolase[†,‡]

Patricia M. Legler,[§] Desigan Kumaran,[||] Subramanyam Swaminathan,[||] F. William Studier,[||] and Charles B. Millard*[,§]

Division of Biochemistry, Walter Reed Army Institute of Research, Silver Spring, Maryland 20910, and Biology Department, Brookhaven National Laboratory, Upton, New York 11973

Received May 27, 2008; Revised Manuscript Received July 8, 2008

ABSTRACT: *Saccharomyces cerevisiae* expresses a 67.8 kDa homodimeric serine thioesterase, *S*-formylglutathione hydrolase (SFGH), that is 39.9% identical with human esterase D. Both enzymes possess significant carboxylesterase and *S*-formylglutathione thioesterase activity but are unusually resistant to organophosphate (OP) inhibitors. We determined the X-ray crystal structure of yeast (y) SFGH to 2.3 Å resolution by multiwavelength anomalous dispersion and used the structure to guide site-specific mutagenesis experiments addressing substrate and inhibitor reactivity. Our results demonstrate a steric mechanism of OP resistance mediated by a single indole ring (W197) located in an enzyme "acyl pocket". The W197I substitution enhances ySFGH reactivity with paraoxon by >1000-fold ($k_i^{W197I} = 16 \pm 2$ mM^{-1} h^{-1}), thereby overcoming natural OP resistance. W197I increases the rate of OP inhibition under pseudo-first-order conditions but does not accelerate OP hydrolysis. The structure of the paraoxon-inhibited W197I variant was determined by molecular replacement (2.2 Å); it revealed a stabilized sulfenic acid at Cys60. Wild-type (WT) ySFGH is inhibited by thiol reactive compounds and is sensitive to oxidation; thus, the cysteine sulfenic acid may play a role in the regulation of a "D-type" esterase. The structure of the W197I variant is the first reported cysteine sulfenic acid in a serine esterase. We constructed five Cys60/W197I variants and show that introducing a positive charge near the oxyanion hole, W197I/C60R or W197I/C60K, results in a further enhancement of the rates of phosphorylation with paraoxon ($k_i = 42$ or 80 mM^{-1} h^{-1}, respectively) but does not affect the dephosphorylation of the enzyme. We also characterized three histidine substitutions near the oxyanion hole, G57H, L58H, and M162H, which significantly decrease esterase activity.

Human esterase D (hEstD),[1] also called *S*-formylglutathione hydrolase (SFGH, EC 3.1.2.12) (*1*), is a ubiquitous intracellular carboxylesterase (CE). hEstD can be found in blood cells and most human tissues (*2*) and is one of the major CE activities detectable in cytosolic fractions of human liver (*3*). SFGH hydrolyzes a range of uncharged ester substrates *in vitro*, including *p*-nitrophenyl acetate (pNPA) and 4-methylumbelliferyl acetate. Clinical screening of SFGH/hEstD activity was useful in linkage studies aimed at locating a retinoblastoma locus on chromosome 13 (reviewed in ref *4*). hEstD has more recently been found to be selectively overexpressed in at least one invasive breast cancer cell line (*5*). On the basis of results obtained *in vitro* and *in vivo* (*6, 7*), it is widely accepted that SFGH functions as a thioesterase in the removal of genotoxic formaldehyde via a glutathione-dependent reaction (Scheme 1). The enzyme may also play a role in xenobiotic metabolism (*8*), as SFGH can be induced in human cells by exposure to methylmethane sulfonate or phenobarbital (*2, 9*).

Saccharomyces cerevisiae SFGH (ySFGH) and hEstD are "D-type" esterases as originally defined by Main (*10*) because they are susceptible to inhibition by Hg^{2+} but are resistant to organophosphorus (OP) inhibitors such as paraoxon [diethyl *p*-nitrophenyl phosphate (DEP)]. The classification of these enzymes as either serine or thiol esterases remained unclear prior to the X-ray crystal structure of the *S. cerevisiae* SFGH (PDB entry 1PV1), which confirmed the catalytic triad, Ser161-His276-Asp241 (amino acid numbering of

[†] This work was funded by the U.S. Defense Threat Reduction Agency JSTO Award 1.D0015_06_WR_C (C.B.M.), by the Protein Structure Initiative of the National Institutes of Health as part of the New York Structural Genomics Research Consortium, and by the Office of Biological and Environmental Research of the U.S. Department of Energy.

[‡] The atomic coordinates of the ySFGH crystal structures have been deposited in the Protein Data Bank as entries 1PV1 (wild type) and 3C6B (W197I variant).

* To whom correspondence should be addressed: Division of Biochemistry, 503 Robert Grant Ave., Silver Spring, MD 20910-7500. Telephone: (301) 319-9506. Fax: (301) 319-9150. E-mail: charles.b.millard@us.army.mil.

[§] Walter Reed Army Institute of Research.

[||] Brookhaven National Laboratory.

[1] Abbreviations: AChE, acetylcholinesterase; AEBSF, 4-(2-aminoethyl)benzenesulfonyl fluoride HCl; BChE, butyrylcholinesterase; bME, β-mercaptoethanol; CD, circular dichroism; CE, carboxylesterase; DEP, diethyl *p*-nitrophenylphosphate; DMP, dimethyl *p*-nitrophenylphosphate; DMSO, dimethyl sulfoxide; DTT, dithiothreitol; hEstD, human esterase D; IPTG, isopropyl β-thiogalactoside; MAD, multiwavelength anomalous dispersion; MALDI-TOF, matrix-assisted laser desorption ionization time-of-flight mass spectrometry; MSE, selenomethionine; NCS, noncrystallographic symmetry; OP, organophosphate; PMSF, phenylmethanesulfonyl fluoride; pNPA, *p*-nitrophenyl acetate; pNPB, *p*-nitrophenyl butyrate; rmsd, root-mean-square deviation; SDS−PAGE, sodium dodecyl sulfate−polyacrylamide gel electrophoresis; SFGH, *S*-formylglutathione hydrolase; TS, transition state; WT, wild type; y, yeast.

10.1021/bi8010016 CCC: $40.75
Published on Web 08/16/2008

Scheme 1: Formaldehyde Detoxification[a]

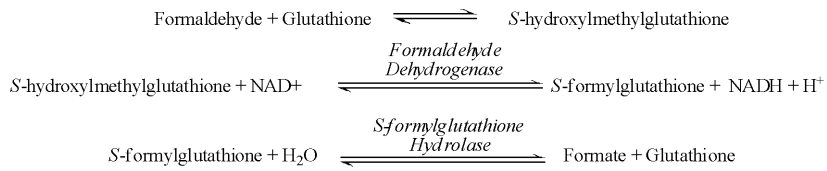

[a] *S*-Hydroxymethylglutathione is spontaneously formed from the reaction of formaldehyde and glutathione. *S*-Formylglutathione is the product of formaldehyde dehydrogenase, an enzyme which catalyzes the oxidation of *S*-hydroxymethylglutathione. SFGH catalyzes the hydrolysis of *S*-formylglutathione to produce formate and glutathione. Formate is then oxidized to carbon dioxide by formate dehydrogenase, and glutathione is recycled in subsequent detoxification reactions.

1PV1 used throughout), and pointed to a conserved cysteine adjacent to the triad (Cys60) in the regulation of the enzyme. Negligible losses of SFGH activity in a C60S variant (*11*), however, have confounded the role of the conserved cysteine in catalysis.

While the chemistry and structural features underlying OP reactive serine esterases are well-documented, relatively little is known of the OP resistance mechanism of D-type esterases. Understanding the molecular basis for OP resistance and susceptibility is of toxicological interest as these inhibitors are used as pesticides as well as therapeutics (reviewed in refs *12* and *13*).

At least three possible mechanisms could account for the apparent SFGH resistance to organophosphorus inhibitors: (1) poor binding of the OP, for example, by steric exclusion from the active site (*14*); (2) poor chemical reactivity, which may be caused by inefficient accommodation of the OP transition state (TS) (*15*); or (3) rapid OP hydrolase activity, since enzymes which hydrolyze OP are not irreversibly inhibited (*16, 17*). On the basis of analysis of a recently determined crystal structure of *Arabidopsis thaliana* SFGH, Cummins et al. postulated a steric exclusion mechanism (due to an acyl pocket residue) for resistance of SFGH to PMSF based upon a predicted clash between the inhibitor and an acyl pocket residue. Superposition of a structurally related enzyme inhibited by DEP (*18*) onto ySFGH also suggests steric exclusion. By a combined application of site-directed mutagenesis, X-ray crystallography, and inhibition and reactivation kinetics, we determine the mechanism of OP resistance for a eukaryotic D-type esterase and examine the role of the cysteine adjacent to the triad in inhibition and reactivation.

We determined the X-ray crystal structure of a ySFGH variant (W197I) following phosphorylation with DEP (PDB entry 3C6B described herein) which enabled the assignment of the oxyanion hole residues. The introduction of an imidazolium near the oxyanion hole of selected α/β-serine hydrolases enhances OP hydrolase activity (*16, 19*), but this strategy has not been tested on a D-type esterase or in enzymes which are structurally dissimilar to cholinesterase or human CE1. SFGH has an uncommon fold and an unusual regulatory cysteine. In a preliminary attempt to determine if OP hydrolase activity could be enhanced in the SFGH scaffold, we constructed three histidine variants and measured OP inhibition and reactivation rates. As an alternative approach, we constructed a series of amino acid substitutions (His, Gln, Lys, and Arg) at residue Cys60 located within 4−9 Å of the oxyanion hole to examine the effects of a positive charge on organophosphorus reactivity at this position. While characterizing and reversing the natural OP resistance of SFGH enzymes, we trapped an unexpected sulfenic acid which suggests a potential regulatory role for Cys60 in D-type esterases.

EXPERIMENTAL PROCEDURES

Materials. BugBuster was from Novagen (San Diego, CA). G-75 Sephadex, Q-Sepharose, and PD-10 columns were from GE Healthcare Life Sciences (Piscataway, NJ). BioSpin-6 columns were from Bio-Rad (Hercules, CA). QuikChange kits were purchased from Stratagene (La Jolla, CA). All substrates were from Sigma. Neat dimethyl *p*-nitrophenylphosphate (DMP) and DEP were from ChemServices Inc. (West Chester, PA) and were 99% pure; phenylmethanesulfonyl fluoride (PMSF) and 4-(2-aminoethyl)benzenesulfonyl fluoride HCl (AEBSF) were from Sigma (St. Louis, MO). Detailed procedures for the cloning, expression, and purification of ySFGH and its mutants are supplied as Supporting Information.

Esterase Assays. CE activity was routinely measured using *p*-nitrophenyl acetate (pNPA) or butyrate (pNPB) dissolved in dimethyl sulfoxide (DMSO). pNP was monitored at 405 nm and room temperature (22 ± 2 °C) in 0.067 M Na/K phosphate (Sorensen's buffer) (pH 7.4). Hydrolysis of *S*-lactoylglutathione was monitored at 240 nm (ε = 3100 M^{-1} cm^{-1}) (*20*). The protein concentration was determined by using the absorbance at 280 nm, a calculated ε of 56060 M^{-1} cm^{-1}, and a molecular mass of 33934 Da. A unit was defined as a micromole of product produced per minute. Enzyme stock solutions contained 2−4 mM bME and were diluted 1:100 in all assays.

Inhibition Kinetics. Progressive inhibition by DMP, DEP, or PMSF was assessed in the absence of substrate with at least four different concentrations of inhibitor (in DMSO) essentially as described in ref *21*. The K_p is analogous to a Michaelis constant, where k_2 is the maximum rate of inhibition at a saturating inhibitor concentration.

$$k_{obs} = k_2/(1 + K_p/[I]) \quad (1)$$

The apparent bimolecular rate constant for inhibition, k_i, describes the rate of formation of the covalent E−I complex from free enzyme and inhibitor in the absence of substrate and was calculated according to eq 2.

$$k_i = k_2/K_p \quad (2)$$

Reactivation Kinetics. The rate of spontaneous reactivation, or the return of pNPA hydrolysis activity over time due to spontaneous hydrolysis of the inhibitor from the active site

Table 1: X-ray Crystallography Data Collection and Refinement Summary Statistics

Data Collection and Processing				
	ySFGH (1PV1)			
	remote	edge	peak	DEP-W197I (3C6B)
space group	$P2_12_12_1$			$C2$
unit cell dimensions (Å)	$a = 121.4$, $b = 66.9$, $c = 171.9$			$a = 57.9$, $b = 69.0$, $c = 79.0$, $\alpha = \gamma = 90°$, $\beta = 92.6$
wavelength (Å)	0.9300	0.9791	0.9787	1.54
resolution range (Å)[a]	50−2.3 (2.38−2.30)			80−2.2 (2.26−2.17)
no. of unique reflections	56795 (4702)	50447 (3215)	56213 (4549)	16188 (855)
R_{sym}[b]	0.079 (0.49)	0.065 (0.39)	0.083 (0.56)	0.14 (0.31)
$I/\sigma I$	10.8 (1.8)	9.8 (1.4)	10.3 (1.6)	11.13 (2.2)
completeness	86.7 (69.4)	74 (42.3)	86.1 (67.5)	97.8 (82.8)
redundancy	14.2	9.8	13.5	5.1
no. of Se atoms	12			
phasing power (iso/ano)[c]		1.28/2.44	1.38/2.57	

Refinement Statistics		
	ySFGH (1PV1)	DEP-W197I (3C6B)
resolution (Å)	500−2.3	80−2.2
no. of reflections	53832	15361
R_{factor}[d]	0.255	0.190
R_{free}[e]	0.298 (5%)[d]	0.252 (5%)[d]
no. of atoms		
protein	9340	2311
solvent	122	63
other		8
average B factor (Å^2)		
protein	29.8	12.8
solvent	23.8	8.2
rmsd from ideal geometry		
bond lengths (Å)	0.01	0.024
bond angles (deg)	1.61	2.06
Ramachandran plot		
most favored regions (%)	81.9	87.9
additional allowed regions (%)	14.4	10.5
generously allowed regions (%)	2.6	1.2
disallowed regions (%)	1.1	0.4 (Ser161)

[a] Values in parentheses are for the outermost data shell. [b] $R_{sym} = \sum|I_i - \langle I\rangle|/\sum I_i$. [c] Phasing power = $\langle F_H\rangle/E$(iso) or $\langle 2F''(\text{cal})\rangle/E$(ano); defined in SHARP. [d] R_{factor} for the working set of reflections was calculated using the equation $R_{factor} = \sum||F_o| - |F_c||/\sum|F_o|$. [e] R_{free} for a test set and the size of the test set as the percentage of total reflections in parentheses.

serine, was measured essentially as described previously (*16, 22*). Inhibitors were removed with BioSpin-6 columns in triplicate or single PD-10 columns. Fractions were incubated at 37 °C for 40−100 h. The removal of inhibitor was verified by mixing the fractions with a dilute solution of acetylcholinesterase (AChE) from *Torpedo californica* (*23*). No significant decreases (<20%) in activity were observed. Identical columns were run using uninhibited enzyme. The percent reactivation was plotted over time and fit to the following equation (*24*):

$$v_i = v_u(1 - e^{-k_{obs}t}) \quad (3)$$

where v_i is the activity of the inhibitor-treated enzyme column fraction and v_u is the activity of the uninhibited enzyme incubated at 37 °C for the same length of time.

Crystallization of ySFGH. The Se-Met ySFGH enzyme was crystallized under Hampton Cryo Screen condition number 10 [0.17 M ammonium acetate, 0.085 M sodium acetate trihydrate (pH 4.6), 25.5% (w/v) PEG 4000, and 15% glycerol] in sitting drops consisting of equal volumes of precipitant and protein solution (~7 mg/mL protein stock). Thick crystalline plates were obtained after a few weeks at 17 ± 2 °C.

Crystals of the ySFGH W197I variant were prepared using the same precipitant. ySFGH W197I was fully inhibited by DEP at 22 ± 2 °C prior to crystallization. Excess inhibitor was removed with a Superdex G-200 column [50 mM Tris (pH 7.6), 150 mM NaCl, and 2 mM bME]. Suitable crystals were selected after 3 months and flash-frozen in liquid nitrogen.

Structure Determination and Refinement. The structure of the ySFGH selenomethionine derivative was determined by multiple-wavelength anomalous dispersion (MAD) methods (*25*). Three data sets at peak, edge, and remote wavelengths were collected at the X12C beamline of the National Synchrotron Light Source using a Brandeis CCD detector. Data collection statistics are listed in Table 1. Patterson maps were calculated, and the positions of 12 Se atoms were obtained using PHASES and SOLVE (*26*). Fractional positions of the Se atoms were refined and the phases computed with SHARP (*25*). Phases were improved further using noncrystallographic symmetry (NCS) and solvent flattening. Maps calculated from the data collected at the remote wavelength were used for model building. Iterative rounds of model refinement were performed using O (*27*) and the maximum likelihood target function of CNS 1.1 (*28*).

Diffraction data for crystals of the ySFGH W197I variant were collected with a Bruker FR591 high-flux, rotating anode X-ray diffractometer (PROTEUM) and a SMART 6000 2K CCD detector at WRAIR. Initial phases were calculated from

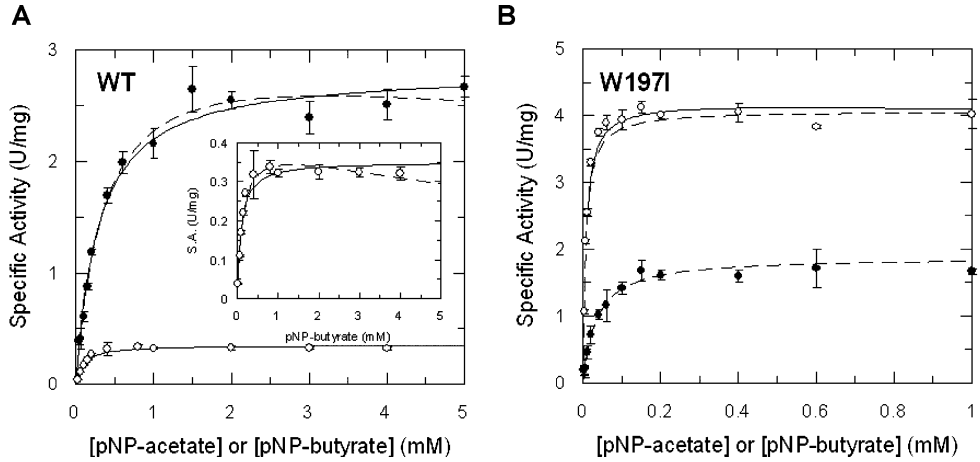

FIGURE 1: Steady-state kinetics of WT and W197I ySFGH. (A) The WT enzyme shows substrate preference for pNPA (●) over pNPB (○). In all graphs, the solid line shows the data fit to the Michaelis−Menten equation; the dotted line shows the data fit to the Haldane equation [$v = V_{max}/(1 + K_m/s + s/K_{ss})$]. The absorbance at 405 nm was monitored in Sorensen's buffer (pH 7.4) at 22 °C. Error bars show standard deviations from at least three measurements. Below 5 mM, pNP acetate substrate inhibition was not observed ($k_{cat} = 107 \pm 8$ min^{-1}, $K_m = 0.5 \pm 0.2$ mM, $K_{ss} = 10 \pm 10$ mM). The inset shows an enlargement of the pNP butyrate data and fits. (B) The substrate preference is reversed in the W197I variant. Substrate inhibition was not observed with either substrate below 1 mM.

1PV1, and the structure was determined by molecular replacement using Amore (*29*). Simulated annealing was carried out with CNS (*28*). The model was refined using Coot 0.1.2 and Refmac5 (*30*).

Thermal Denaturation Curves. Thermal denaturation was monitored (2 °C/min) from 45 to 80 °C using a Jasco 810 circular dichroism spectrophotometer fitted with a Peltier temperature controller. The melting temperature was determined from a four-parameter fit of the averaged ellipticity at 222 nm versus temperature from at least two variable-temperature scans conducted at the same protein concentration.

RESULTS AND DISCUSSION

Purification and Characterization of S. cerevisiae SFGH. ySFGH was overexpressed in *Escherichia coli* and purified to a single band in a Coomassie-stained SDS−PAGE gel (≥95% pure). The identity of the protein was verified by mass spectrometry (Table 1 of the Supporting Information). The elution of a 56.9−62.4 kDa dimer from a calibrated G-75 Sephadex column confirmed that WT ySFGH dimers are present in solution. The kinetic constants of pNPA hydrolysis by ySFGH purified by the protocol described above (Figure 1 and Table 2) are comparable to those reported for endogenous ySFGH purified from *S. cerevisiae* (*7*). The substrate preference for pNPA over pNPB and the resistance to DEP and sensitivity to thiol alkylating agents are in keeping with the operational definition of a D-type esterase (*10*). The reported specificity constant for *S*-formylglutathione is 31-fold higher than that measured for pNPA (*7*). For WT ySFGH, the rate of hydrolysis of *S*-lactoylglutathione (*S*-LG) was not significantly above the spontaneous rate of hydrolysis at the highest substrate concentration tested (1.25 mM) (Table 2).

Wild-Type ySFGH Can Be Slowly Inhibited by High Concentrations of DMP and DEP. While other groups have been unable to show that WT ySFGH can be inhibited by DEP (*11, 31*), we were able to measure inhibition using millimolar concentrations of OP. WT ySFGH can be inhibited by high concentrations of either DMP or DEP to >95% at 22 ± 2 °C and pH 7.4 (Table 3 and Figure 2A).

Table 2: Steady-State Kinetic Parameters for ySFGH-Catalyzed Hydrolysis of *S*-Lactoylglutathione (*S*-LG), *p*-Nitrophenyl Acetate (pNPA), or *p*-Nitrophenyl Butyrate (pNPB) for the WT and Variants Described Herein[a]

enzyme	substrate	K_m (mM)	k_{cat} (min^{-1})	k_{cat}/K_m (mM^{-1} min^{-1})
WT	pNPA	0.40 ± 0.07	108 ± 7	270 ± 50
	pNPB	0.09 ± 0.02	11.9 ± 0.3	130 ± 30
	S-LG[b]	>1.25		
W197I	pNPA	0.054 ± 0.006	63 ± 2	1200 ± 100
	pNPB	0.04 ± 0.01	115 ± 7	2900 ± 700
	S-LG	3 ± 1	7000 ± 2000	2000 ± 1000
M162H	pNPA	0.9 ± 0.4	6 ± 1	7 ± 3
	pNPB	0.14 ± 0.05	0.19 ± 0.01	1.4 ± 0.5
C60S	pNPA[c]	0.32 ± 0.06	95 ± 3	300 ± 60
	pNPA	0.19 ± 0.03	92 ± 3	480 ± 80
	pNPB	0.09 ± 0.03	4.7 ± 0.3	50 ± 20
C60Q/W197I	pNPA	0.10 ± 0.01	31.5 ± 0.6	320 ± 30
	pNPB	0.012 ± 0.002	99 ± 3	8000 ± 1000
C60H/W197I	pNPA	0.34 ± 0.03	90 ± 2	260 ± 20
	pNPB	0.13 ± 0.02	218 ± 9	1700 ± 300
C60K/W197I	pNPA	0.15 ± 0.01	58.3 ± 0.9	390 ± 30
	pNPB	0.03 ± 0.02	74 ± 6	2500 ± 1600
C60R/W197I	pNPA	0.013 ± 0.002	19.0 ± 0.3	1500 ± 200
	pNPB	0.018 ± 0.03	26 ± 1	1400 ± 200
C60S/W197I	pNPA	0.14 ± 0.01	45.8 ± 0.7	330 ± 20
	pNPB	0.019 ± 0.002	118 ± 3	6200 ± 700
	S-LG	3 ± 2	3000 ± 1000	1000 ± 700
M162H/C60S/W197I	pNPA	2.6 ± 0.9	1.7 ± 0.3	0.7 ± 0.2
	pNPB	0.12 ± 0.03	2.4 ± 0.1	20 ± 5
L58H/W197I	pNPA[d]	0.23 ± 0.07	0.33 ± 0.03	1.5 ± 0.5
	pNPB[d]	≤0.2	≤0.99	≤5

[a] Assays were conducted in Sorensen's buffer at pH 7.4 and 22 ± 2 °C, and parameters were determined from nonlinear curve fits to the Michaelis−Menten equation unless stated otherwise. [b] Activity was not twice above background. [c] Measured after bME had been removed from the enzyme stock solution. [d] Derived from Lineweaver−Burke extrapolation instead of direct curve fit.

The *O*-alkyl groups of DMP and DEP differ by only a methylene group; the K_p of DEP ($K_p^{DEP} = 29 \pm 9$ mM) is 12-fold higher than that measured for DMP ($K_p^{DMP} = 2.5 \pm 0.9$ mM). The reactions of WT ySFGH with OP inhibitors are relatively slow compared to those of several other serine esterases, including AChE, butyrylcholinesterase (BChE), hCE-1, or hCE2 (e.g., DMP $k_i = 72000$ mM^{-1} h^{-1} for human AChE) (*32, 33*). In fact, the phosphorylation rates of WT ySFGH are more comparable with those of the serine-protease α-chymotrypsin (e.g., DEP $k_i = 0.3$ mM^{-1} h^{-1}) (*34*).

Table 3: Kinetic Parameters of Phosphorylation (k_2, K_p, and k_i) and Spontaneous Reactivation (k_{obs}, % reactivation) for ySFGH and Its Mutants Inhibited with DMP or DEP[a]

	k_2 (h^{-1})	K_p (mM)	k_i (h^{-1} mM^{-1})	k_{obs} (h^{-1})	% reactivation
			Methyl Paraoxon (DMP)		
WT	0.29 ± 0.03	2.5 ± 0.9	0.12 ± 0.04	0.8 ± 0.2	29 ± 9
C60S				0.20 ± 0.04	35 ± 2
M162H	13 ± 8	200 ± 100	0.07 ± 0.05	0.4 ± 0.2	16 ± 2
W197I	25 ± 4	3.5 ± 0.8	7 ± 2	0.21 ± 0.04	50 ± 5
W197I/C60S	N/D			0.17 ± 0.02	13.7 ± 0.4
W197I/C60Q	14.4 ± 0.7	5 ± 1	2.9 ± 0.6	0.25 ± 0.06	20 ± 2
W197I/C60H	32 ± 8	4 ± 2	8 ± 4	0.09 ± 0.05	13 ± 1
W197I/C60K	38.2 ± 0.7	2.3 ± 0.3	17 ± 2	0.24 ± 0.09	7 ± 1
W197I/C60R	48 ± 6	5 ± 1	10 ± 2	0.15 ± 0.03	18 ± 1
			Paraoxon (DEP)		
WT	0.4 ± 0.1	29 ± 9	0.014 ± 0.005		
W197H	6.0 ± 0.2	0.38 ± 0.05	16 ± 2		
W197I	11.2 ± 0.5	0.7 ± 0.1	16 ± 2	N/D	<4
W197I/C60Q	19 ± 1	1.1 ± 0.3	17 ± 5	N/D	<5
W197I/C60H	20 ± 3	0.8 ± 0.6	30 ± 20	N/D	<1
W197I/C60K	46 ± 5	0.6 ± 0.2	80 ± 30	N/D	<2
W197I/C60R	44 ± 2	1.04 ± 0.09	42 ± 4	N/D	<1

[a] Inhibition rates were measured at room temperature (22 ± 2 °C) in Sorensen's buffer with 2 mM bME (pH 7.4); spontaneous reactivation was assessed at 37 °C in the same buffer.

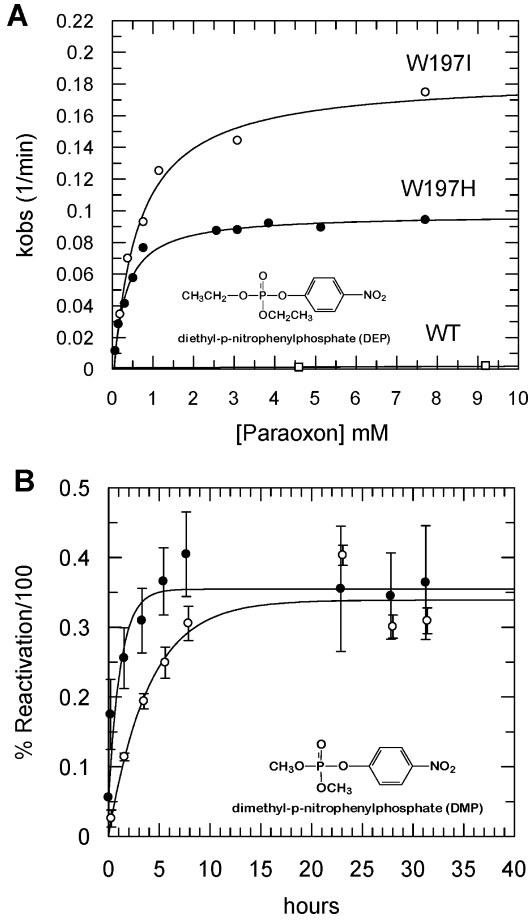

FIGURE 2: Inhibition and reactivation of WT ySFGH and site-directed mutants. (A) Dependence of k_{obs} on the concentration of DEP for the WT (□), W197H (●), and W197I (○) variants fitted to eq 1 (*21*). Only two of the four points are shown for the WT enzyme in this graph. Enzymes were inhibited in Sorensen's buffer (pH 7.4) and 2 mM bME at 22 °C. (B) Spontaneous reactivation after DMP inhibition of WT (●) and C60S (○) at 37 °C collected in triplicate. Standard deviations are shown. In both cases, approximately half of the enzyme was reactivated. Rates of reactivation are reported in Table 3.

The slower rate of inhibition in ySFGH is partly due to the acyl pocket, which may limit the binding of inhibitors containing acyl groups larger than a methyl group and/or poorly accommodate the pentacoordinate TS of these inhibitors. The faster rate of phosphorylation in human AChE may also be due to its three-point oxyanion hole versus the two-point oxyanion hole of ySFGH.

To confirm that OP resistance was not due to OP hydrolase activity, we measured the rate of spontaneous reactivation of the DMP adduct of the WT enzyme (k_{obs} = 0.8 ± 0.2 h^{-1}). At pH 7.4 and 37 °C, less than half of the enzyme is reactivated (29 ± 9%) (Figure 2B). On the basis of the slow rates of spontaneous reactivation, we ruled out natural OP resistance due to accelerated OP hydrolase activity.

Structure of SFGH (1PV1). Crystals diffracted beyond 2.2 Å and belonged to the $P2_12_12_1$ space group; the structure was refined to 2.3 Å resolution (Table 1). The overall topology of ySFGH reveals an infrequent variant within the α/β-hydrolase superfamily, supporting an earlier sequence-based prediction that the sequence YJLO68C might encode a novel fold (*35, 36*). ySFGH is built around a three-layer sandwich architecture with an uncommon nine-stranded β-sheet and eight helices, three of which (residues 124−142, 161−178, and 278−296) are bent (30−45°) (Figure 3A).

WT ySFGH crystallized as a dimer of dimers with four molecules in the asymmetric unit (Figure 3B). The interface between chains A and B is estimated to be 3300 Å^2 by AreaMol and corresponds to ~$^1/_4$ of the overall surface area (~11100 Å^2). Although ySFGH contains five Cys residues, the monomers and dimers do not possess disulfide bonds; all of the Cys residues appear to be in the reduced state in 1PV1.

Catalytic Triad. ySFGH contains a Ser161/His276/Asp241 catalytic triad (Figure 4A) in a conserved ^{159}GHSMG^{163} motif. The serine is in a strained conformation (ϕ and ψ angles of 52.6−60.0° and −103.5° to −105.3°, respectively), making the Ser-OH or "nucleophilic elbow" well exposed to His276. The active site of ySFGH (PDB entry 1PV1) is occupied by a large (>10σ) spherical peak within hydrogen bonding distance of the putative oxyanion hole residues, Leu58 and Met162; the density may represent partial occupancy of a solvent anion.

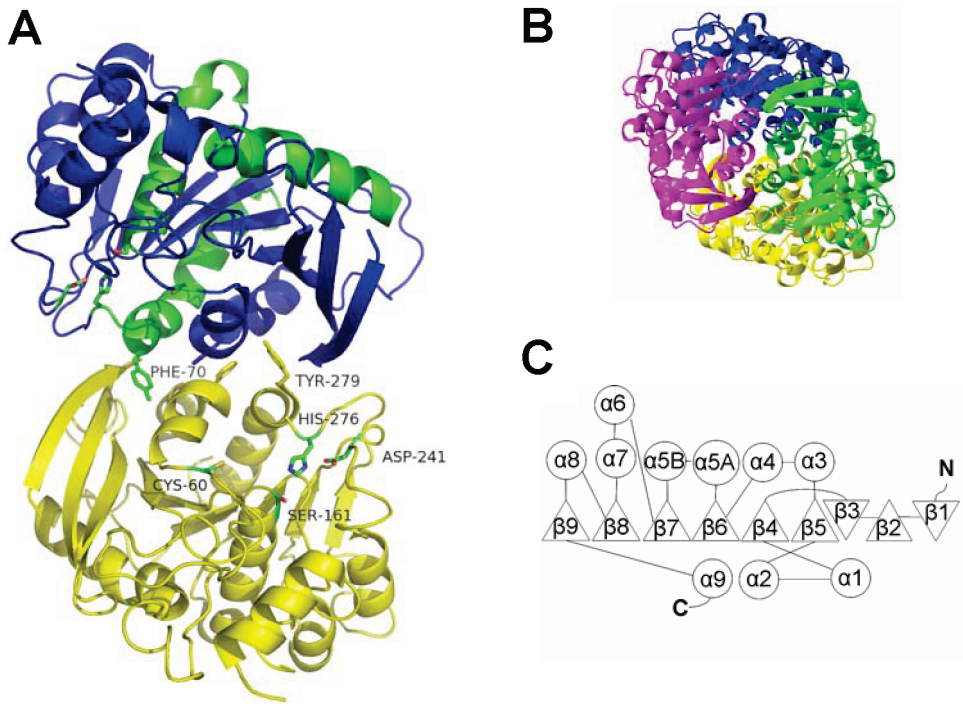

FIGURE 3: Structure of *S. cerevisiae* SFGH determined at 2.3 Å (1PV1). (A) Structure of the ySFGH homodimer. At the dimer interface, the side chain of Tyr279 inserts into the opposing monomer. (B) Structure of the dimer of dimers found in the asymmetric unit. (C) Topology of ySFGH [diagram generated by TOPS (*47*)]. Helices 4, 5, and 9 (colored green in panel A) are significantly bent; each half of helix 5 is diagramed as two helices (α5A and α5B). Panels A and B were generated using PyMOL (DeLano Scientific, LLC).

Structural Similarity. The *A. thaliana* SFGH enzyme was reported to share a topology with 1PV1 (cf., Figure 3C and ref *11*). The plant SFGH is not currently available in the protein database, but a Dali structural similarity search (*37*) identifies antigen 85C, a mycolyltransferase from *Mycobacterium tuberculosis*, as another close structural neighbor of SFGH (PDB entry 1DQY) (*18*). The structure of antigen 85C is similar to that of ySFGH (overall rmsd of 2.3 Å over 209 C_α atoms with 1PV1) despite a low level of sequence identity (17%). The 85C fold, however, contains only eight β-strands.

Antigen 85C contains a Ser/His/Glu triad like most serine esterases (*38*) and can be inhibited by DEP in 12 h at 4 °C with a roughly 2-fold molar excess (*18*). Residues adjacent to the alkyl group of the octyl thioglucoside substrate of antigen 85C differ significantly between the two enzymes. Another significant difference is the presence of Arg41 near the active site serine in antigen 85C, a residue which is replaced with Thr59 in ySFGH. Antigen 85C does not contain a Cys near its active site; an Ala is located at the homologous position.

Acyl Pocket. The superposition of 3C6B with 1PV1 suggests that the acyl pocket is primarily formed by the hydrophobic residues L58, W102, I189, F243, L248, and W197. In the WT enzyme, the shallow acyl pocket most likely accounts for the high substrate specificity for the small formyl group of *S*-FG (*7*). On the basis of a superposition of ySFGH and DEP-inhibited antigen 85C, we expressed and purified a W197I variant to enhance OP reactivity.

Effects of the W197I Acyl Pocket Substitution on Substrate Specificity. Trp197 limits the depth of the acyl pocket (Figure 1A,B of the Supporting Information). The W197I substitution increases the specificity constant for *S*-LG and pNPB (22-fold) (Table 2) and inverts the substrate preference (Figure 1). The W197I substitution primarily affects the turnover numbers for the *S*-LG substrate (which increases from undetectable to 7000 ± 2000 mM^{-1} min^{-1}) and pNPB substrate (9.7-fold increase) and has an only small ~2-fold effect on the K_m (pNPB). The observed increase in k_{cat} may reflect a faster on-rate due to a more open active site.

Effects of W197I Acyl Pocket Substitution on OP Reactivity. Preferences for substrates are recapitulated in the specificity constants of the DMP and DEP inhibitors. The W197I substitution enhances the rate of DMP inhibition 60-fold when compared to that of WT ySFGH (Table 3). The effect is primarily on k_2 which increases by 2 orders of magnitude when compared to that of WT. A <2-fold increase in K_p is observed. The rate enhancement may be due to better accommodation of the transition state and/or faster on-rates.

Unlike WT ySFGH, the W197I variant is readily inhibited by DEP ($k_i^{WT\text{-}DEP} = 0.014 \pm 0.005$ h^{-1} mM^{-1} vs $k_i^{W197I\text{-}DEP} = 16 \pm 2$ h^{-1} mM^{-1}) and PMSF (Table 2 of the Supporting Information). The 3 order of magnitude rate enhancement is due to both a 40-fold decrease in K_p and a 28-fold increase in k_2. Comparable inhibition rates are observed for the W197I and W197H variants with DEP (Figure 2A); both substitutions effectively abolish OP resistance by enlarging the acyl pocket. OP resistance in WT ySFGH appears to be primarily due to steric occlusion by a single indole ring in the acyl pocket but may also be attributed to poor accommodation of the TS of the OP since the W197I substitution affects both K_p and k_2.

While the W197I substitution increases the apparent phosphorylation rate constant, the spontaneous reactivation rate (dephosphorylation) of DMP-inhibited W197I is similar to that of WT ySFGH; only partial reactivation of the W197I variant (50 ± 5%) is observed as with WT (29 ± 9%). In

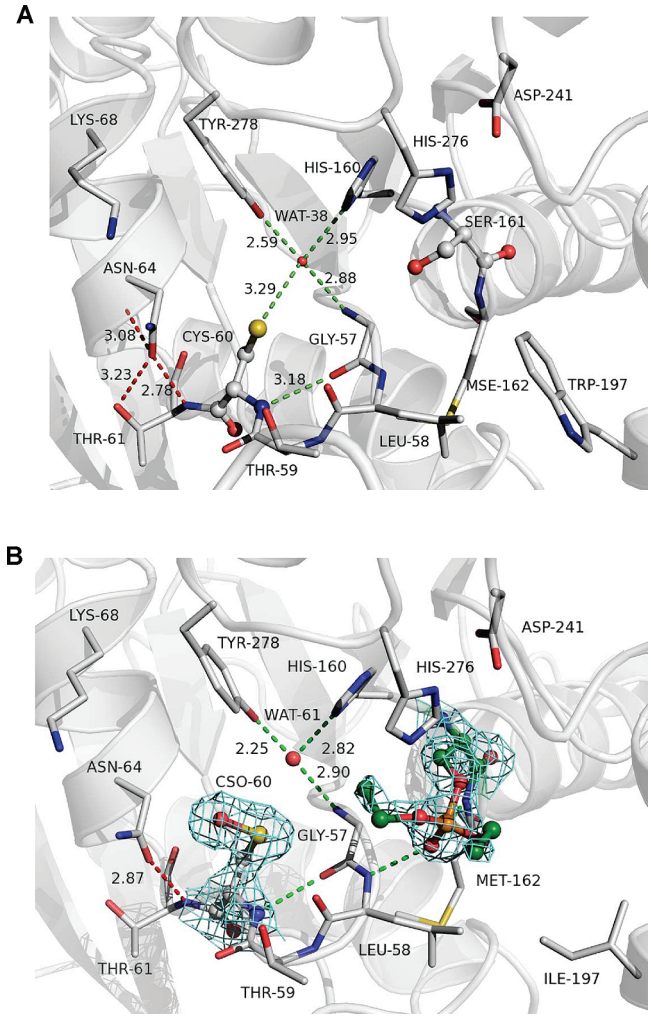

FIGURE 4: Active site of WT ySFGH and the W197I variant. (A) The Ser161/His276/Asp241 catalytic triad and adjacent Cys60 are shown in the structure of WT ySFGH (PDB entry 1PV1). MSE refers to selenomethionine. (B) Active site of the W197I variant showing density for the covalently bound DEP at the 1.5σ contour level (PDB entry 3C6B). Positive and negative density is not visible at the $\pm 4\sigma$ contour level. The oxyanion hole is formed by the backbone amide NH group of Leu58 and Met162. The H-bonding distances from the phosphoryl oxygen of DEP to the backbone amide groups of Leu58 and Met162 are 2.7 and 3.1 Å, respectively. An oxidized Cys60 sulfenic acid was also trapped in this structure. The hydrogen bonding interaction between the Asn64 carbonyl and Thr61 backbone NH groups which most likely prevents the formation of a cyclic sulfenamide is colored red. This figure was generated using PyMOL (DeLano Scientific, LLC).

contrast, after DEP inhibition, only a very small amount of the W197I enzyme is reactivated (<4%). The C60S substitution has no significant effect on the spontaneous rate of reactivation in the W197I/C60S double mutant after DMP inhibition ($k_{obs} = 0.17 \pm 0.02$ h^{-1}). Only partial reactivation (13.7 ± 0.4%) occurs after 50 h, 3-fold less than with the W197I variant.

We compared the melting temperatures, measured by CD, of the uninhibited and inhibited W197I variant to determine if incomplete reactivation was due to DEP-induced unfolding of the enzyme. The DEP modification of W197I increases the observed T_m by 6 °C when compared to that of the unmodified enzyme (Table 3 of the Supporting Information). Similar stabilization for other OP enzyme complexes has been observed and attributed to favorable enthalpic interactions between the OP and residues of the enzyme active site. Slow and incomplete enzyme reactivation following DEP inhibition may have been caused by the stabilizing effects of nearby residues on the OP−Ser bond, as well as post-inhibitory processes that compete with dephosphorylation (*39*). These processes may include denaturation after phosphorylation and/or dephosphorylation, or more complex reaction mechanisms such as the loss of an alkyl group from the OP via enzyme-catalyzed side reactions (cf., cholinesterase "aging" reaction). Denaturation was ruled out by the observed increase in the measured T_m by CD. The nitrogen of His276 (2.9 Å) of the catalytic triad in the 3C6B structure is closer to the oxygen of the DEP *O*-ethyl group than the O_γ atom of Ser161 (3.4 Å). The H-bond to the *O*-alkyl group is a common feature of other aged structures (*40, 41*) and may prevent deprotonation of the attacking water or protonation of the leaving Ser161 by His276 during dephosphorylation.

Structure of the W197I Acyl Pocket Variant. W197I-DEP crystallized in space group *C*2 and diffracted to 2.1 Å; data from the 2.2 Å resolution shell were included for refinement. Strong positive difference electron density (>12σ), tetrahedral in shape, in the initial $F_o - F_c$ maps corresponded with the OP in a covalent bond with the O_γ atom of Ser161 (Figure 2A of the Supporting Information and Figure 4B). Electron density for the ethoxy groups was relatively weak, consistent with their enhanced rotational mobility; similar density has been reported for other DEP structures (*18, 42*).

Positive difference electron density (>9.5σ) at Cys60 was best modeled as a cysteine sulfenic acid (Figure 2 of the Supporting Information and Figure 4B). Attempts to model a sulfinic acid or hydrosulfonyl group [−S(OH)═O or O═S(H)═O] into the density resulted in positive and/or negative density. While oxidation to the sulfenic acid can be reversed by reductants such as glutathione, the sulfinic acid or sulfone cannot be reversibly reduced (*43*). All other cysteines were in the reduced state.

Large conformational changes were not observed between the structures of the WT enzyme and DEP-W197I; the two structures could be superimposed with a root-mean-square deviation (rmsd) of 0.50 Å over 288 C_α atoms. In both 1PV1 and 3C6B, two phenylalanine residues (Phe70 and Phe73) at the A−B dimer interface appear disordered as evidenced by increased thermal factors for these side chains.

Oxyanion Hole. The DEP structure allows us to unambiguously assign the oxyanion hole of SFGH. It is formed by two potential H-bonds from the backbone amide groups of Met162 (O···H−N bond distance of 3.1 Å) and Leu58 (O···H−N bond distance of 2.9 Å) to the phosphoryl oxygen of DEP (Figure 4B and Scheme 2). The structure supports the assignment of the backbone amides made by Cummins et al. in *A. thaliana* SFGH and argues against the mechanism of Gonzales et al. (*20*), which proposes that the backbone amides of Gly159 and Ser161 of 1PV1 function as the oxyanion hole residues. In the structure of 3C6B, the Ser161 amide is 5.3 Å from the double-bonded phosphoryl oxygen and is thus an unlikely oxyanion hole residue. Similarly, the Gly159 NH group is located in a β-strand 11 Å from the phosphoryl oxygen.

Effects of Oxyanion Hole Substitutions on Esterase Activity and OP Hydrolysis. Mutation of oxyanion hole residues has led to significant rate enhancements in the dephosphorylation

Scheme 2: Proposed Mechanism for the Hydrolysis of *S*-Formylglutathione under Reducing Conditions

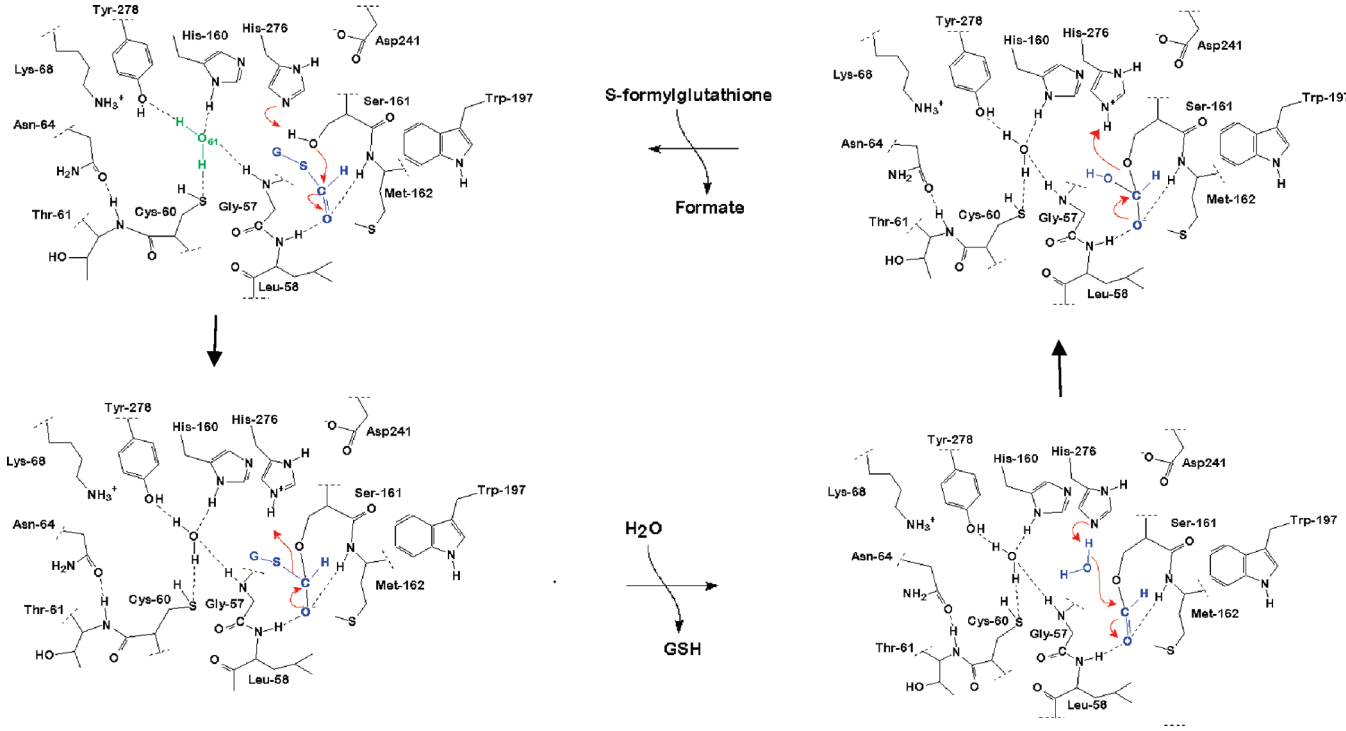

of OP adducts from human BChE and *Bungarus fasciatus* AChE (*16, 22*). While OP hydrolase activity has been engineered into enzymes which share the cholinesterase fold by the conversion of a single Gly residue in the oxyanion hole to a His (*16*), ySFGH was not amenable to the analogous substitution. Substitution of G57, L58, and M162 with histidine in attempts to mimic the role of G117H in BChE decreased the rate of pNPA hydrolysis by at least 1 order of magnitude (Table 2), suggesting that the active site substitutions interfered with the formation of the pNPA TS and/or binding of the substrate. Purified G57H/W197I did not have detectable levels of pNPA hydrolysis above background consistent with a steric clash (Figure 1C of the Supporting Information). The L58H and M162H substitutions were sufficiently far from the active site serine and were not expected to interfere directly with catalysis. However, only the M162H variant retained activity near that of the WT enzyme, and no increase in the reactivation rate after inhibition by DMP was observed (Table 3).

Cysteine Subsite. D-Type esterases have been shown to be inhibited by sulfhydryl reactive compounds such as NEM, Hg^{2+}, and iodoacetamide (*2, 11*). Cummins et al. proposed that alkylation of Cys60 leads to a steric blockade of the active site. A C60Q variant exhibited a 2-fold decrease in pNPA activity comparable to that reported for iodoacetamide; however, the K_m did not significantly increase in the C60Q/W197I double mutant when compared to that of W197I, suggesting that the substitution does not affect substrate binding.

Effects of Cys60 Substitutions on Esterase Activity. To determine if a positively charged residue at this position could act as an additional electrostatic catalyst in OP hydrolysis, we constructed a series of Cys60/W197I double mutants. The Cys60 substitutions had only modest effects on the k_{cat} and K_m of pNP substrates when compared with those of W197I; the specificity constants were within a factor of 5 (Table 2). The C60H/W197I double mutant had the largest observed increase in K_m (6-fold, pNPA) and k_{cat} (1.4-fold) and the largest decrease in its specificity constant (4.6-fold). Significant changes in K_m were not observed for the variants with more flexible side chains; therefore, this does not suggest steric effects in substrate binding. The nearby positive charge may instead affect the nucleophilicity of the active site serine since reductions in k_{cat} were observed as the side chain length increased (C60H > C60K > C60R).

Effects of Cys60 Substitutions on OP Reactivity. Mutating Cys60 to Q, H, K, or R had small but significant effects on OP reactivity. Rates of DEP phosphorylation quadrupled in the C60K and C60R/W197I double mutants when compared to that of the W197I variant (Table 3), suggesting that the substitutions primarily affect the transition state. Only minor effects on K_p were observed (<2-fold different from that of W197I). It is unlikely that the longest side chain, R60, H-bonds with the OP (Figure 1D of the Supporting Information) since Lys could effectively replace Arg at the same position.

The T_m of the C60S/W197I double mutant was not significantly different from that of W197I, suggesting only a minor role for Cys60 in hydrophobic packing. With the C60K and C60R/W197I substitutions, the T_m decreased by 11 and 10 °C, respectively, suggesting that the charged residue may alter hydrophobic packing and/or promote aggregation.

Trapping the Cys60 Sulfenic Acid in the DEP-Inhibited W197I Variant. Little insight into the role of Cys60 in modulating the activity of SFGH in the presence of oxidizing or alkylating reagents has been reported. Although other explanations cannot be excluded, the sulfenic acid found only at Cys60 suggests a regulatory role under oxidizing conditions (reviewed in ref *43*). The structure of 3C6B is the first report of a sulfenic acid in a serine esterase. The sulfur atom of Cys60 in 3C6B is 3.3 Å (3.5−3.7 Å in 1PV1) from the

Gly57 carbonyl oxygen which is adjacent to the Leu58 NH group that is part of the oxyanion hole. The angle among Cβ, Sγ, and the carbonyl oxygen of Gly57 is nearly 90° and is too acute to enable a hydrogen bonding interaction. The electron density maps do not show evidence of a cyclic sulfenamide (*44*); a 2.9 Å hydrogen bonding interaction between the Asn64 side chain carbonyl oxygen and the Thr61 NH group most likely precludes its formation (Figure 4). Deprotonation of the sulfur is required for sulfenic acid formation. Hydrogen peroxide or superoxide-mediated oxidation of the sulfhydryl to yield the sulfenic acid can occur by at least two mechanisms: (1) nucleophilic attack on peroxide by a thiolate anion (*45*) due to a lowered sulfhydryl pK_a or (2) abstraction of a hydrogen atom (H$^\bullet$) from the sulfhydryl by a radical, resulting in a thiyl radical (S$^\bullet$) directly above the G57−L58 peptide bond; reaction with oxygen or another hydroxyl radical would form the neutral R−SO$^\bullet$ or R−SOH species (*46*). The observed acceleration of OP inhibition of the C60H, C60K, and C60R variants suggests that a positive charge at this position accelerates the phosphorylation step. Similarly, the increase in the k_{cat} of the C60H/W197I double mutant suggests that a positive charge above the peptide bond shared by the oxyanion hole residue Leu58 can enhance the acylation step; thus, a negatively charged thiolate, sulfenate, or sulfinate anion may slow the reaction. Trapping the sulfenic acid during or after OP inhibition suggests that its formation may be coupled to catalysis. Additional experiments are needed to identify the pathway by which the sulfenic acid is formed and to determine whether the sulfenic acid itself is inhibitory or protective (against overoxidation).

ACKNOWLEDGMENT

We thank Benjamin V. Clingan, Christian Eusebio, Sue Ellen Gerchman, and Helen Kycia for technical assistance. We thank Dr. Albert S. Mildvan for useful discussions and helpful suggestions.

SUPPORTING INFORMATION AVAILABLE

Surface maps of the WT and W197I active sites, models of the variants described, OMIT maps, inhibition kinetics with PMSF, melting temperatures, mass spectrometry data, and cloning and purification procedures. This material is available free of charge via the Internet at http://pubs.acs.org.

REFERENCES

1. Eiberg, H., and Mohr, J. (1986) Identity of the polymorphisms for esterase D and S-formylglutathione hydrolase in red blood cells. *Hum. Genet. 74*, 174–175.
2. Lee, W. H., Wheatley, W., Benedict, W. F., Huang, C. M., and Lee, E. Y. (1986) Purification, biochemical characterization, and biological function of human esterase D. *Proc. Natl. Acad. Sci. U.S.A. 83*, 6790–6794.
3. Crow, J. A., Borazjani, A., Potter, P. M., and Ross, M. K. (2007) Hydrolysis of pyrethroids by human and rat tissues: Examination of intestinal, liver and serum carboxylesterases. *Toxicol. Appl. Pharmacol. 221*, 1–12.
4. Cowell, J. K. (1989) One hundred years of retinoblastoma research. From the clinic to the gene and back again. *Ophthalmic Paediatr. Genet. 10*, 75–88.
5. Jessani, N., Humphrey, M., McDonald, W. H., Niessen, S., Masuda, K., Gangadharan, B., Yates, J. R., III, Mueller, B. M., and Cravatt, B. F. (2004) Carcinoma and stromal enzyme activity profiles associated with breast tumor growth in vivo. *Proc. Natl. Acad. Sci. U.S.A. 101*, 13756–13761.
6. Harms, N., Ras, J., Reijnders, W. N., van Spanning, R. J., and Stouthamer, A. H. (1996) S-Formylglutathione hydrolase of *Paracoccus denitrificans* is homologous to human esterase D: A universal pathway for formaldehyde detoxification? *J. Bacteriol. 178*, 6296–6299.
7. Degrassi, G., Uotila, L., Klima, R., and Venturi, V. (1999) Purification and properties of an esterase from the yeast *Saccharomyces cerevisiae* and identification of the encoding gene. *Appl. Environ. Microbiol. 65*, 3470–3472.
8. Cashman, J. R., Perotti, B. Y., Berkman, C. E., and Lin, J. (1996) Pharmacokinetics and molecular detoxication. *Environ. Health Perspect. 104* (Suppl. 1), 23–40.
9. Jelinsky, S. A., and Samson, L. D. (1999) Global response of *Saccharomyces cerevisiae* to an alkylating agent. *Proc. Natl. Acad. Sci. U.S.A. 96*, 1486–1491.
10. Main, A. R. (1960) The differentiation of the A-type esterases in sheep serum 1. *Biochem. J. 75*, 188–195.
11. Cummins, I., McAuley, K., Fordham-Skelton, A., Schwoerer, R., Steel, P. G., Davis, B. G., and Edwards, R. (2006) Unique regulation of the active site of the serine esterase S-formylglutathione hydrolase. *J. Mol. Biol. 359*, 422–432.
12. Costa, L. G. (2006) Current issues in organophosphate toxicology. *Clin. Chim. Acta 366*, 1–13.
13. Millard, C. B., and Broomfield, C. A. (1995) Anticholinesterases: Medical applications of neurochemical principles. *J. Neurochem. 64*, 1909–1918.
14. Kovarik, Z., Radic, Z., Berman, H. A., Simeon-Rudolf, V., Reiner, E., and Taylor, P. (2003) Acetylcholinesterase active centre and gorge conformations analysed by combinatorial mutations and enantiomeric phosphonates. *Biochem. J. 373*, 33–40.
15. Cui, F., Qu, H., Cong, J., Liu, X. L., and Qiao, C. L. (2007) Do mosquitoes acquire organophosphate resistance by functional changes in carboxylesterases? *FASEB J.,* 3584–3591.
16. Millard, C. B., Lockridge, O., and Broomfield, C. A. (1995) Design and expression of organophosphorus acid anhydride hydrolase activity in human butyrylcholinesterase. *Biochemistry 34*, 15925–15933.
17. Newcomb, R. D., Campbell, P. M., Ollis, D. L., Cheah, E., Russell, R. J., and Oakeshott, J. G. (1997) A single amino acid substitution converts a carboxylesterase to an organophosphorus hydrolase and confers insecticide resistance on a blowfly. *Proc. Natl. Acad. Sci. U.S.A. 94*, 7464–7468.
18. Ronning, D. R., Klabunde, T., Besra, G. S., Vissa, V. D., Belisle, J. T., and Sacchettini, J. C. (2000) Crystal structure of the secreted form of antigen 85C reveals potential targets for mycobacterial drugs and vaccines. *Nat. Struct. Biol. 7*, 141–146.
19. Lockridge, O., Blong, R. M., Masson, P., Froment, M. T., Millard, C. B., and Broomfield, C. A. (1997) A single amino acid substitution, Gly117His, confers phosphotriesterase (organophosphorus acid anhydride hydrolase) activity on human butyrylcholinesterase. *Biochemistry 36*, 786–795.
20. Gonzalez, C. F., Proudfoot, M., Brown, G., Korniyenko, Y., Mori, H., Savchenko, A. V., and Yakunin, A. F. (2006) Molecular basis of formaldehyde detoxification. Characterization of two S-formylglutathione hydrolases from *Escherichia coli*, FrmB and YeiG. *J. Biol. Chem. 281*, 14514–14522.
21. Kitz, R., and Wilson, I. B. (1962) Esters of methanesulfonic acid as irreversible inhibitors of acetylcholinesterase. *J. Biol. Chem. 237*, 3245–3249.
22. Poyot, T., Nachon, F., Froment, M. T., Loiodice, M., Wieseler, S., Schopfer, L. M., Lockridge, O., and Masson, P. (2006) Mutant of *Bungarus fasciatus* acetylcholinesterase with low affinity and low hydrolase activity toward organophosphorus esters. *Biochim. Biophys. Acta 1764*, 1470–1478.
23. Millard, C. B., Lockridge, O., and Broomfield, C. A. (1998) Organophosphorus Acid Anhydride Hydrolase Activity in Human Butyrylcholinesterase: Synergy Results in a Somanase. *Biochemistry 37*, 237–247.
24. Hovanec, J. W., and Lieske, C. N. (1972) Spontaneous reactivation of acetylcholinesterase inhibited with para-substituted phenyl methylphosphonochloridates. *Biochemistry 11*, 1051–1056.
25. De La Fortelle, E., and Bricogne, G. (1997) Maximum-likelihood heavy atom parameter refinement in the MIRE and MAD methods. *Methods Enzymol. 276*, 472–493.
26. Furey, W., and Swaminathan, S. (1997) PHASES-95: A Program Package for the Processing and Analysis of Diffraction Data from Macromolecules. *Methods Enzymol. 277*, 590–620.
27. Jones, T. A., Zou, J. Y., Cowan, S. W., and Kjeldgaard, M. (1991) Improved methods for building protein models in electron density

maps and the location of errors in these models. *Acta Crystallogr. A47* (Part 2), 110–119.
28. Brünger, A. T., Adams, P. D., Clore, G. M., DeLano, W. L., Gros, P., Grosse-Kunstleve, R. W., Jiang, J. S., Kuszewski, J., Nilges, M., Pannu, N. S., Read, R. J., Rice, L. M., Simonson, T., and Warren, G. L. (1998) Crystallography & NMR system: A new software suite for macromolecular structure determination. *Acta Crystallogr. D54*, 905–921.
29. Navaza, J. (2001) Implementation of molecular replacement in AMoRe. *Acta Crystallogr. D57*, 1367–1372.
30. Collaborative Computational Project, Number 4 (1994) The CCP4 suite: Programs for protein crystallography. *Acta Crystallogr. D50*, 760–763.
31. Uotila, L., and Koivusalo, M. (1974) Purification and properties of S-formylglutathione hydrolase from human liver. *J. Biol. Chem. 249*, 7664–7672.
32. Worek, F., Diepold, C., and Eyer, P. (1999) Dimethylphosphoryl-inhibited human cholinesterases: Inhibition, reactivation, and aging kinetics. *Arch. Toxicol. 73*, 7–14.
33. Maxwell, D. M., and Brecht, K. M. (2001) Carboxylesterase: Specificity and spontaneous reactivation of an endogenous scavenger for organophosphorus compounds. *J. Appl. Toxicol. 21* (Suppl. 1), S103–S107.
34. Hartley, B. S., and Kilby, B. A. (1950) Inhibition of chymotrypsin by diethyl p-nitrophenyl phosphate. *Nature 166*, 784–785.
35. Sánchez, R., and Sali, A. (1998) Large-scale protein structure modeling of the *Saccharomyces cerevisiae* genome. *Proc. Natl. Acad. Sci. U.S.A. 95*, 13597–13602.
36. Burley, S. K., Almo, S. C., Bonanno, J. B., Capel, M., Chance, M. R., Gaasterland, T., Lin, D., Sali, A., Studier, F. W., and Swaminathan, S. (1999) Structural genomics: Beyond the human genome project. *Nat. Genet. 23*, 151–157.
37. Orengo, C. A., Michie, A. D., Jones, S., Jones, D. T., Swindells, M. B., and Thornton, J. M. (1997) CATH: A hierarchic classification of protein domain structures. *Structure 5*, 1093–1108.
38. Cygler, M., Schrag, J. D., Sussman, J. L., Harel, M., Silman, I., Gentry, M. K., and Doctor, B. P. (1993) Relationship between sequence conservation and three-dimensional structure in a large family of esterases, lipases, and related proteins. *Protein Sci. 2*, 366–382.
39. Thompson, C. M. (1992) Consequence of phosphorus stereochemistry upon the postinhibitor reaction kinetics of acetylcholinesterase poisoned by phosphorothiolates. *J. Am. Chem. Soc. 114*, 10710–10715.
40. Bencsura, A., Enyedy, I., and Kovach, I. M. (1995) Origins and diversity of the aging reaction in phosphonate adducts of serine hydrolase enzymes: What characteristics of the active site do they probe? *Biochemistry 34*, 8989–8999.
41. Millard, C. B., Kryger, G., Ordentlich, A., Greenblatt, H. M., Harel, M., Raves, M. L., Segall, Y., Barak, D., Shafferman, A., Silman, I., and Sussman, J. L. (1999) Crystal structures of aged phosphonylated acetylcholinesterase: Nerve agent reaction products at the atomic level. *Biochemistry 38*, 7032–7039.
42. Nachon, F., Asojo, O. A., Borgstahl, G. E., Masson, P., and Lockridge, O. (2005) Role of water in aging of human butyrylcholinesterase inhibited by echothiophate: The crystal structure suggests two alternative mechanisms of aging. *Biochemistry 44*, 1154–1162.
43. Claiborne, A., Yeh, J. I., Mallett, T. C., Luba, J., Crane, E. J., III, Charrier, V., and Parsonage, D. (1999) Protein-sulfenic acids: Diverse roles for an unlikely player in enzyme catalysis and redox regulation. *Biochemistry 38*, 15407–15416.
44. Yang, J., Groen, A., Lemeer, S., Jans, A., Slijper, M., Roe, S. M., den Hertog, J., and Barford, D. (2007) Reversible oxidation of the membrane distal domain of receptor PTPα is mediated by a cyclic sulfenamide. *Biochemistry 46*, 709–719.
45. Denu, J. M., and Tanner, K. G. (1998) Specific and reversible inactivation of protein tyrosine phosphatases by hydrogen peroxide: Evidence for a sulfenic acid intermediate and implications for redox regulation. *Biochemistry 37*, 5633–5642.
46. Carballal, S., Alvarez, B., Turell, L., Botti, H., Freeman, B. A., and Radi, R. (2007) Sulfenic acid in human serum albumin. *Amino Acids 32*, 543–551.
47. Michalopoulos, I., Torrance, G. M., Gilbert, D. R., and Westhead, D. R. (2004) TOPS: An enhanced database of protein structural topology. *Nucleic Acids Res. 32*, D251–D254.

BI8010016